Experimental Study for Polarimetric Measurement of Non-specular Wave Scattering from Building Surface Roughness

Hary Budiarto,Kenshi Horihata, Katsuyuki Haneda and Jun-ichi Takada
Tokyo Institute of Technology
2-12-1 Ookayama Meguro-ku Tokyo Japan 152-8552
email: hary@ap.ide.titech.ac.jp,haneda@ap.ide.titech.ac.jp, takada@ide.titech.ac.jp

***Abstract*— This paper presents polarimetric measurement of non-specular scattering from building surface roughness based on experimental data. Both V-V and V-H polarizations were estimated independently. The superresolution method was applied as an approach to handle signal parameters of the individual incoming waves scattered from building surface roughness. In order to comprehend the details of microscopic mechanisms of the scattering, signal parameters shall be incorporated into multiple scattering approach based on ray optics.**

***Index Terms*— Polarimetric, Non-specular Scattering, Multipath Propagation, ESPRIT**

I. Introduction

In urban areas, buildings are the dominant scatterers determining radio propagation properties. Reflection, diffraction, transmission and scattering of the electromagnetic waves on the building surfaces in the radio environment induce undesirable multipath propagation. Consequently, the transmitted signal reaches the receiver through different propagation paths. On the other hand, polarization rotation or cross polarization directly adversely affect in the performance of polarization diversity. The prediction of multipath on the building surface that includes polarization effect will be beneficial for the radio propagation models [7]. The multipath propagation characteristics of non-specular wave scattering from building surface roughness have been reported in other papers [1][2][3][4]. This paper presents experimental study for polarimetric measurement of non-specular wave scattering from building surface roughness. The estimation of the vertical-vertical (V-V) and vertical-horizontal (V-H) polarizations were carried out independently. Signal parameters from the polarizations of the individual incoming waves scattered from building surface roughness were obtained using the superresolution method. The experimental results show that the non-specular scattering from building surface is more dominated by window frames scatterers rather than brick scatterers. The average path gain difference between V-V and V-H polarizations was 12 dB. This is consistent between measurement by using Vector Network Analyzer and signal parameters estimated by using the superresolution method (Least Square 3D Unitary ESPRIT).

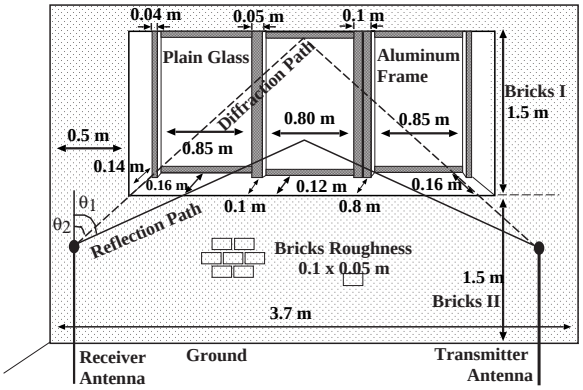

Fig. 1. Building Surface Profile

II. Environment Under Consideration

A. Building Surface Profile

The profile of the building surface is shown in Fig. 1. The profile was taken from one of the buildings at Tokyo Institute of Technology. The surface of the building has non-uniformity due to the windows (glass), frames (aluminum), and walls (bricks). The surface has periodical irregularity of five periods. One period of the surface equals 3.7 m. The windows are made up of the sidewall, aluminum frames and plain glasses, which in principle are the building roughness, as well as the wall surface. The dimensions of the window's glasses of the building are 0.85×1.5 m^2, 0.8×1.5 m^2, and 0.85×1.5 m^2. The three different window frames have outer dimensions of 0.04×1.5 m^2, 0.05×1.5 m^2 and 0.10×1.5 m^2. The first and the third window frames have the same offset depth of 0.16 m different from the second window frame that has 0.12 m offset depth. The windows are elevated 1.5 m from the ground. The wall surface, that has periodical roughness in both horizontal and vertical directions, is made of 0.1×0.05 m^2 bricks with 0.01 m gap among each other.

B. Transmitter and Receiver Model

Rectangular microstrip antennas, which are polarized linearly, were used as both transmitter and receiver antennas. The ground plane size is 0.08×0.08 m^2 and the patch size is 0.0179×0.0179 m^2 on a dielectric substrate with

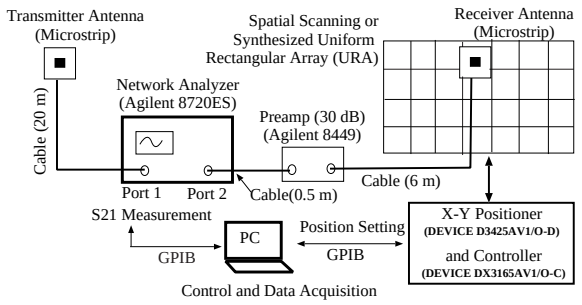

Fig. 2. Equipment Arrangement

$\epsilon_r = 2.55$. Frequency of the antennas was 4.85-5.05 GHz. The wavelength was comparable with or smaller than the depth of building surface roughness. The height of the transmitter antenna was 1.9 m. The transmitter and receiver antennas were fixed at 2.7 m in front of the building surface. The antennas were aligned to transmit and receive the V-V followed by V-H polarizations. Figure 2 shows equipment arrangement for transmitter and receiver model. During the experiment, the V-V and V-H polarizations were measured independently under the same environment. The measurement of V-H polarization were conducted by rotating the receiver antenna -90° toward the right direction of the receiver when it was in V-V polarization. The measured cross-polarization discrimination (XPD) of the antenna is around 20 dB in an anechoic chamber. The transfer function between transmitter and receiver antennas were measured using a vector network analyzer (VNA). Measurement of transfer function and the shifting of receiver antenna were operated automatically using a personal computer connected to the controller of the x-y positioner through the General Purpose Interface Bus (GPIB), in order to attain high accuracy and easy measurement. The X-Y positioner is used for automatically shifting the receiver antenna with spatial scanning accuracy of 1 mm. Table 1 shows the detailed parameters of the experiments.

C. The Spatial Scanning Model

The spatial scanning was configured to resemble an array antenna, also called synthesized uniform rectangular array (URA). The measurement points during the spatial scanning were discretized for every 0.025 m toward the horizontal and vertical directions. The measurement was performed along 0.5 m in the vertical direction. The middle of the vertical direction scanning region was at the same height as the transmitter antenna. Figure 3 illustrates model of the spatial scanning. The model performs the measurement 8.125 m along the horizontal direction. The transmitter antenna is positioned facing towards the bricks' surface of the building. The first vertical direction of measurement is 0.7 m away from the transmitter antenna, which corresponds to 10° incident angle in the specular direction.

D. Data Measurement Method

Since the VNA measured the transfer function of the cable and amplifier simultaneously, a calibration of the data measurement system was required to eliminate equipment effects. The transfer function measured by the VNA can be expressed as follows,

$$X(f) = H(f) \times G(f) \tag{1}$$

where $G(f)$ is transfer function of the cable, amplifier and antenna complex directivity at broadside, and $H(f)$ is Friis free space transfer function, which is given as,

$$H(f) = \frac{\lambda}{4\pi d} \exp(-j\frac{2\pi}{\lambda}d) \tag{2}$$

where d is propagation path, and λ is wavelength. All measurement data resulted from this experiment were already calibrated by applying function $G(f)$, which was obtained from the measurement using the transmitter and receiver antennas positioned face-to-face with 1 meter distance from each other, in an open space.

Figure 4 shows mean values and standard deviations of data measurement for V-V and V-H polarizations. Mean values and standard deviations were calculated from the vertical spatial scanning. The figure shows them in the errorbar graph with 0.1 m discretized at the horizontal spatial scanning. The average difference between V-V and V-H Polarizations is 12 dB.

TABLE I
EXPERIMENTAL PARAMETER

Antennas	Tx & Rx Microstrip Reflection coefficient is bellow -10 dB in $4.85 - 5.05$ GHz. Beam width in E and H planes are 45°
Measurement Points	Spatially 10×10 points (25 mm interval), 21 points over frequency $(4.85 - 5.05$ GHz).
Snapshot	20 times
Estimations Parameters	The number of waves and each wave's azimuth, elevation, delay and path gain
Signal processing	LS 3-D Unitary ESPRIT
Smoothing in ESPRIT	Spatially 4 times and 7 times over frequency
Wave Polarization	Vertical-Vertical Vertical-Horizontal
Cross-Polarization Discrimination	20 dB
Normalization	Face-to-face, the distance between Tx and Rx is 1 m at experiment location

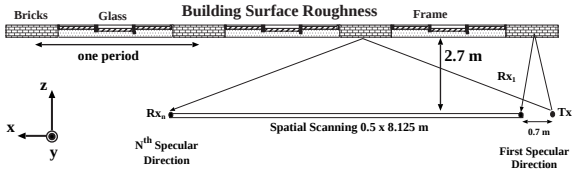

Fig. 3. Top View of the Spatial Scanning Model

III. SIGNAL PROCESSING

In order to obtain signal parameters of the arrival wave, measurement data are formulated. Suppose that L waves are impinging at the receiver have three parameters of azimuth

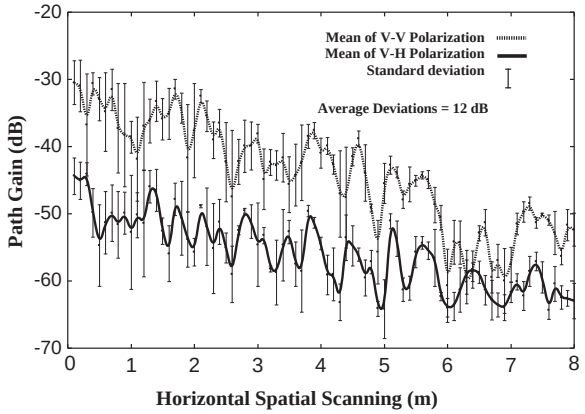

Fig. 4. Means Value and Standard Deviations of Data Measurement for V-V and V-H polarizations

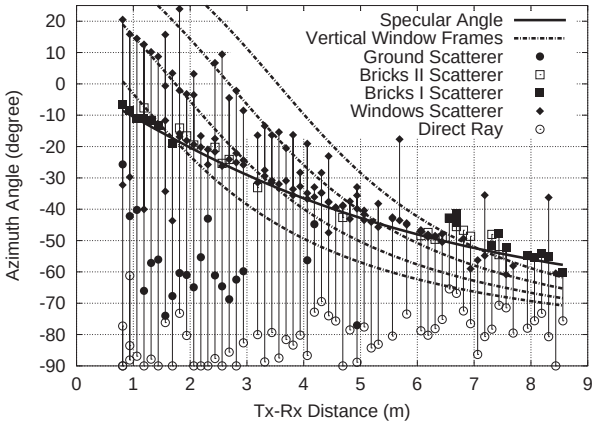

Fig. 5. Azimuth Angle of Arrival Wave for V-V Polarization

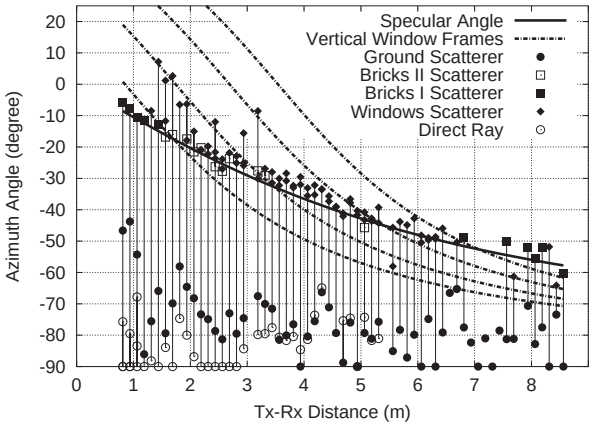

Fig. 6. Azimuth Angle of Arrival Wave for V-H Polarization

angle $(\phi_l - \frac{\pi}{2})$, elevation angle $(\frac{\pi}{2} - \theta_l)$ and delay time τ_l, where $1 \leq l \leq L$. With the X-Y positioner, the receiver antenna performs spatial scanning both in the horizontal and vertical directions where the intervals of the sampling points are Δ_x and Δ_y. The numbers of sampling points are M_1 and M_2, respectively. At each sampling point, it carries out M_3 points of sampling over the frequency where the interval of sampling is Δ_f and the center frequency is f_c. If the electrical lengths of the aperture of the array, $\frac{2\pi}{\lambda_c} M_1 \Delta_x$ and $\frac{2\pi}{\lambda_c} M_2 \Delta_y$, are both sufficient to be assumed as constant within the bandwidth $M_3\Delta_f$, i.e, $M_1\Delta_x \cdot M_3\Delta_f \ll c$, and $M_2\Delta_y \cdot M_3\Delta_f \ll c$, where c is a light velocity, then the measured data y_{k_1,k_2,k_3} can be expressed as,

$$z_{k_1,k_2,k_3} = \sum_{l=1}^{L} \left[s_l \prod_{r=1}^{3} e^{j\mu_l^{(k_r)}} \right] + n_{k_1,k_2,k_3} \tag{3}$$

where $0 \leq k_r \leq (M_r - 1)$ $1 \leq r \leq 3$ indicates a location of each sampling point, n_{k_1,k_2,k_3} is a white Gaussian noise of zero mean, s_l is a complex amplitude of the l^{th} wave at a reference point and $\mu_l^{(r)}$ is denoted by

$$\mu_l^{(1)} = \frac{2\pi}{\lambda_c}\Delta_x \sin(\phi_l - \frac{\pi}{2}) \cos(\frac{\pi}{2} - \theta_l), \tag{4}$$

$$\mu_l^{(2)} = \frac{2\pi}{\lambda_c}\Delta_y \sin(\frac{\pi}{2} - \theta_l), \tag{5}$$

$$\mu_l^{(3)} = 2\pi\Delta_f\tau_l. \tag{6}$$

These values include parameters of the incident waves so that the objective is to obtain these L sets of 3-D mode parameters. Then, vectorization of data measurement can be defined as

$$\begin{aligned} \boldsymbol{z} = [&z_{1,1,1}\ z_{2,1,1} \dots z_{M_1,1,1}\ \ z_{1,2,1} \dots \\ &z_{M_1,M_2,1}\ z_{1,1,2} \dots z_{M_1,M_2,M_3}]^T \in C, \\ &= \boldsymbol{A}\boldsymbol{s} + \boldsymbol{n}, \end{aligned} \tag{7}$$

where $s \in C^L$ and $n \in C^M$ $(M = M_1M_2M_3)$ are the complex amplitude vector and noise vector respectively. The multi-dimensional mode matrix $\boldsymbol{A} \in C^{M\times L}$ is generated by mode matrices each of which corresponds to a parameter as

$$\boldsymbol{A} = \boldsymbol{A}(\mu^{(3)}) \diamond \boldsymbol{A}(\mu^{(2)}) \diamond \boldsymbol{A}(\mu^{(1)}) \in C^{M\times L}, \tag{8}$$

where $\diamond$ denotes the kronecker product of each row of the matrices and

$$\boldsymbol{A}(\mu^{(r)}) = [\boldsymbol{a}(\mu_1^{(r)}) \dots \boldsymbol{a}(\mu_L^{(r)})] \in C^{M_r\times L}, \tag{9}$$

$$a(\mu_1^{(r)}) = [1\ e^{-j\mu_r^{(r)}} \dots e^{-j(M_r-1)\mu^{(r)}}]^T \in C^{M_r}. \tag{10}$$

The 3D unitary ESPRIT algorithm [4][5] was used to obtain the signal parameters. It is a superresolution direction finding method of the arrival wave. In physical terms, the ESPRIT is equivalent to finding out the parameters of the arrival wave using the phase difference between groups of uniformly positioned elements of sensor array. The ESPRIT array data had a size of (10×10) or (25×25) cm^2 for each observation point. The arrival wave analyses were performed at 60 observation points with an interval of 12.5 cm.

IV. Experimental Results

A. Directional Profiles

Figures 4 and 5 show the 3D unitary ESPRIT results for azimuthal angle of the arrival wave for V-V and V-H polarization, respectively. The line perpendicular to the x-axis depicts the range of the azimuthal angle for one observation point. Negative azimuthal angle means the wave is coming from the

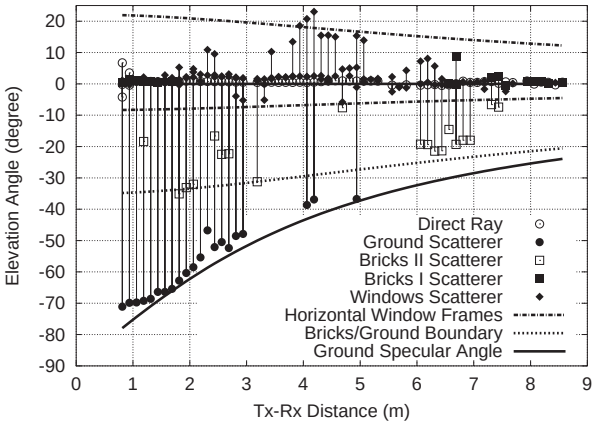

Fig. 7. Elevation Angle of Arrival Wave for V-V Polarization

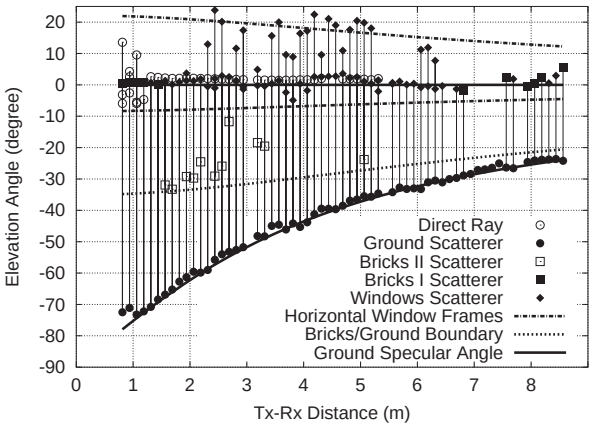

Fig. 8. Elevation Angle of Arrival Wave for V-H Polarization

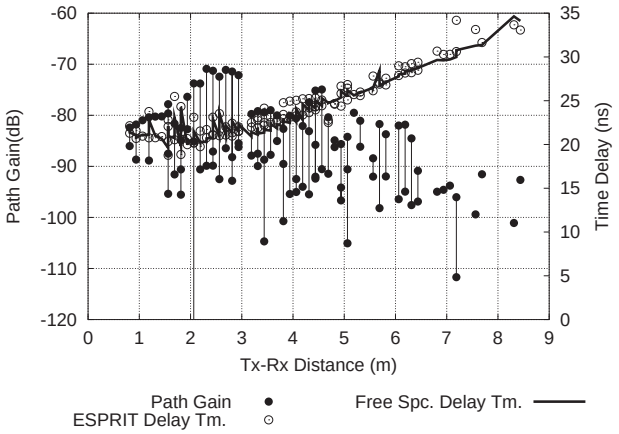

Fig. 9. Power and Delay Time of Arrival Wave for Windows Scatterer with V-V polarization

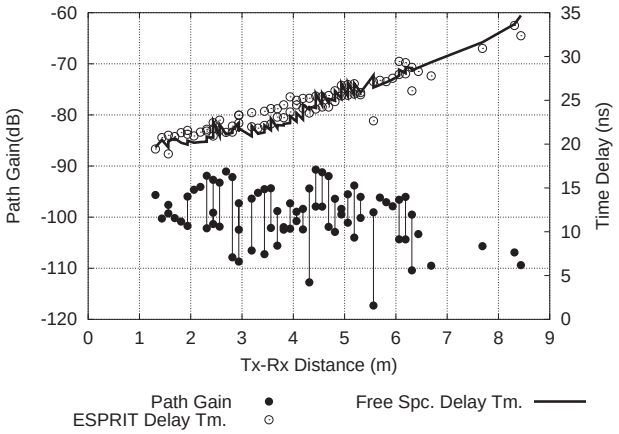

Fig. 10. Power and Delay Time of Arrival Wave for Windows Scatterer with V-H Polarization

right-hand side of the receiver or source side. The legends in figures 4 and 5 show the type of scatterers. The number of legends on the vertical line corresponds to the number of multipath signals. The multipaths can be detected from many scatterers, such as ground, window's glass, window's frame, bricks I, bricks II and directly from the transmitter [3]. The scattering points in the figure are categorized as specular reflection, specular diffraction and diffuse scattering. The specular diffraction that satisfies Keller's law of diffraction can be observed when the scattered waves arrive from vertical frame of the windows. The scatterer wave on the vertical windows frame is dominated by the V-V polarization. Figures 6 and 7 show the elevation angle of the arrival wave for V-V and V-H polarizations, respectively. The diffraction effects are observed when the distance between transmitter and receiver antenna was 3.5-5 m with large elevation angle. It corresponds to horizontal frame of the windows. Likewise, the scatterer wave on the horizontal windows frame is dominated by the V-H polarization. Due to the fact, the V-V polarization has wider spread in azimuth and narrower spread in elevation compared with V-H polarization. Therefore, it can be stated that V-H polarization is concentrated on specular direction for the scattered wave at the building surface. The explanation for this is that frame of windows are the dominant scatterer. Owing to the antenna directivity, the direct wave for V-H polarization and the ground reflected wave for V-V polarization could not be detected at the distance farther than 5 m.

B. Delay Profiles

Figures 8 and 9 show the path gain and delay time of the arrival waves for windows scatterers. When the azimuthal and elevation angles of the arrival wave are known, the propagation path from the transmitter to the receiver antenna can be determined [3]. Therefore, the delay time based on free space velocity (3×10^8 m/s) of each path can be easily obtained. The figures show that the delay time directly estimated by using ESPRIT yields close agreement with the delay time of the propagation path determined by using DoA estimated by ESPRIT and free space velocity. These figures also show that more than one scattered wave from windows (glass and frames) were found for every observation point. This may be due to the shape of windows with slight curvature. Figures 10 and 11 show the path gain and delay time of the arrival waves scattered from bricks I and bricks II. These figures show that the path gain difference between bricks I and bricks II is significant compared with its delay difference even if they are the same material. It is probable that this is caused by diffuse

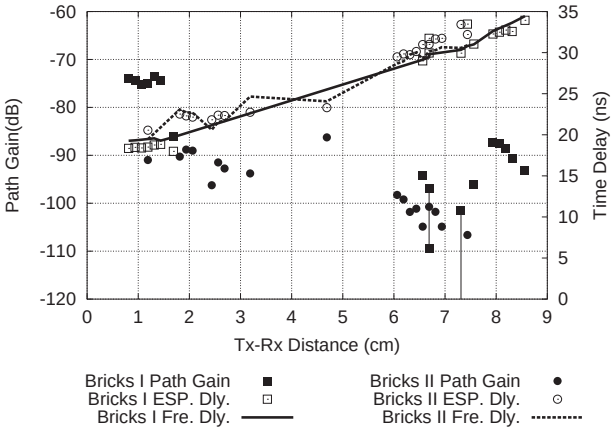

Fig. 11. Power and Delay Time of Arrival Wave for Bricks Scatterer with V-V Polarization

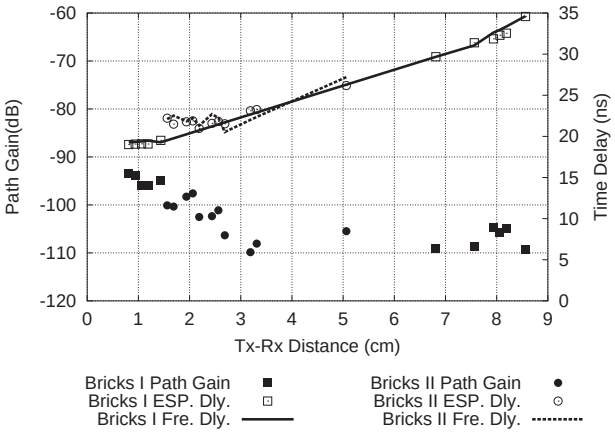

Fig. 12. Power and Delay Time of Arrival Wave for Bricks Scatterer with V-H Polarization

scattering or the reflection coefficient change due to the difference in elevation. The second order scattering from building surface scatterers was not discovered in the V-H polarization. The second order scattering was sometimes found with low path gain and large in delay time. This is proven by the data in table 2 that the delay time for V-H polarization is smaller than V-V polarization. In the V-V and V-H polarization, the non-specular scattering from building surfaces are more dominated by windows frame scatterers rather than brick scatterers. Table 2 shows the average difference of delay time directly estimated by using ESPRIT result and delay time of the propagation path determined by using DoA estimated by ESPRIT and free space velocity. The average of path gain difference between V-V and V-H polarizations was 12 dB. This is consistent with the measurement shown in Fig. 3.

TABLE II
AVERAGE DIFFERENCE OF DELAY TIME AND PATH GAIN

Type	Delay V-V	Delay V-H	Path Gain
Bricks I	0.83 ns	0.26 ns	12.05 dB
Bricks II	0.51 ns	0.24 ns	11.98 dB
Glass	0.62 ns	0.38 ns	11.35 dB

V. CONCLUSION

This paper presents polarimetric measurement of non-specular scattering from building surface roughness. The results show that the non-specular scatterings from building surfaces are more dominated by frame scatterers rather than brick scatterers. The vertical frames are dominant scatterers for V-V polarization. Likewise, the horizontal frames are dominant scatterers for V-H polarization. The second order scattering, which sometimes was found with low path gain and large in delay time, was not discovered in the V-H polarization. The scattering point of the V-V and V-H polarizations can be observed as specular reflection, specular diffraction and diffuse scattering. The average difference of path gain is 12 dB between V-V and V-H polarizations.

REFERENCES

[1] J. Takada, J. Fu, H. Zhu, and T. Kobayashi, “Spatio-Temporal Channel Characterization in a Sub-Urban Non-Line-of-Sight Microcellular Environment”, IEEE J. Select. Areas in Comm., vol. 20, no. 3, pp.532-538, Apr. 2002.

[2] H. Budiarto, K. Horihata, K. Haneda, and J. Takada, “ Superresolution Measurement of Non-specular Wave Scattering from Building Surface Roughness”, Proc. of IEEE VTC Fall 2003 Conf. VII A-3, Orlando-USA.

[3] H. Budiarto, K. Horihata, K. Haneda, and J. Takada,”Experimental study of Non-specular Wave Scattering from Building Surface Roughness for the Mobile Propagation Modeling ”,Accepted to Journal of IEICE Trans. on Communications.

[4] H. Budiarto, K. Horihata, K. Haneda, and J. Takada,”Polarimetric Measurement of Non-specular Wave Scattering from Building Surface Roughness”,Accepted to IEEE Antenna Propagation and Wireless Letter.

[5] K. Sakaguchi, J. Takada and K. Araki, ”A Novel Architecture for MIMO Spatio-Temporal Channel Sounder,” IEICE Transactions on Electronics, vol. E-86C, no. 3, pp. 436-441, Mar. 2002.

[6] M. Haardt and J.A. Nossek, “Simultaneous Schur Decomposition of Several Nonsymmetric Matrices to achieve Automatic pairing in Multidimensional harmonic Retrieval problems”, IEEE Trans. on Signal Processing, vol. 46 no. 1 pp. 161-169, Jan. 1998.

[7] M.O. Al-Nuami and M.S. Ding, “Prediction Models and Measurements of Microwave Signals Scattered from Buildings”, IEEE Trans. on Antenna and Propagation, vol.42, No.8 pp. 1126-1137, August 1994.

[8] H.H. Xia, H.L. Bertoni, L.R. Maciel, A.L. Stewart an R. Rowe, “Radio propagation Characteristic for Line-Of-Sight Microcellular and Personal Communication”, IEEE Trans. on Antenna and Propagation, vol. 41, no.10, pp. 1439-1447, Oct. 1993.

[9] K. Haneda, J. Takada, T. Iwata, and Y. Wakinaka, “Construction of a Propagation Path Determination System for Short Range Wireless Communication System”, in Proc. The 3rd International Workshop on ITS Telecommunications 2002 (ITST 2002), pp 289-294, Seoul, Korea, Nov. 2002.